HHS Public Access

Author manuscript

J Comput Chem. Author manuscript; available in PMC 2016 May 15.

Published in final edited form as:

J Comput Chem. 2015 May 15; 36(13): 970–982. doi:10.1002/jcc.23881.

Comparison of structural, thermodynamic, kinetic and mass transport properties of Mg^{2+} ion models commonly used in biomolecular simulations

Maria T. Panteva, **George M. Giambaşu**, and **Darrin M. York***

Center for Integrative Proteomics Research, BioMaPS Institute and Department of Chemistry & Chemical Biology, Rutgers University, 174 Frelinghuysen Road, Piscataway, NJ 08854-8076, USA

Abstract

The prevalence of Mg^{2+} ions in biology and their essential role in nucleic acid structure and function has motivated the development of various Mg^{2+} ion models for use in molecular simulations. Currently the most widely used models in biomolecular simulations represent a non-bonded metal ion as an ion-centered point charge surrounded by a non-electrostatic pairwise potential that takes into account dispersion interactions and exchange effects that give rise to the ion's excluded volume. One strategy toward developing improved models for biomolecular simulations is to first identify a Mg^{2+} model that is consistent with the simulation force fields that closely reproduces a range of properties in aqueous solution, and then, in a second step, balance the ion-water and ion-solute interactions by tuning parameters in a pairwise fashion where necessary. The present work addresses the first step in which we compare 17 different non-bonded single-site Mg^{2+} ion models with respect to their ability to simultaneously reproduce structural, thermodynamic, kinetic and mass transport properties in aqueous solution. None of the models based on a 12-6 non-electrostatic non-bonded potential was able to reproduce the experimental radial distribution function, solvation free energy, exchange barrier and diffusion constant. The models based on a 12-6-4 potential offered improvement, and one model in particular, in conjunction with the SPC/E water model, performed exceptionally well for all properties. The results reported here establish useful benchmark calculations for Mg^{2+} ion models that provide insight into the origin of the behavior in aqueous solution, and may aid in the development of next-generation models that target specific binding sites in biomolecules.

Keywords

Magnesium; Molecular dynamics; Pairwise potentials; Parametrization; Benchmark

* Electronic address: york@biomaps.rutgers.edu; Corresponding author.

((Additional Supporting Information may be found in the online version of this article.))

Introduction

Magnesium ions are particularly important for nucleic acid systems in stabilizing tertiary structure[1–3], driving folding processes[4–7], and in the case of many ribozymes, playing a direct role in catalysis[8–12]. Due to the biological importance of divalent metal ions, much work has been done, especially in the last decade, to model these ions in molecular simulations[13–16]. As with many computational models, in order to be practical, rigor and complexity must be balanced with computational cost. For simulations of biological systems, care must be taken that the metal ion model keep pace, be balanced and easily integrated with the force field and water model that is being used to represent the rest of the system.

Currently, the most mature and commonly used biomolecular simulation force fields[17–26] are of the static charge, non-polarizable form, and thus not able to explicitly account for multipolar electrostatics or quantum many-body effects[27–33]. Within this class of force fields, there have been two general strategies for constructing metal ion models based on bonded and non-bonded frameworks. Bonded metal ion models use empirical bonding terms to enforce the correct coordination structure, and cannot exchange their ligand environment[34–36]. Non-bonded metal ion models[37], on the other hand, can exchange (at least in principle) in simulations[38], and thus are more general in their potential application to processes where changes in coordination state or binding mode occur. Electrostatic interactions can be modeled in the traditional way with the ionic charge located at the nuclear center, or using multiple sites displaced from the nuclear center. The multi-site models offer greater exibility in distributing charges on the off-center sites, and have demonstrated considerable promise for improving coordination geometries, and selectivity of ion binding[39–43]. Nonetheless, currently the non-bonded models that are most widely used in biomolecular simulations represent a metal ion as an ion-centered point charge surrounded by a non-electrostatic pairwise potential that takes into account dispersion interactions and most signi cantly, exchange effects that give rise to the ion's excluded volume. The most common form for the non-electrostatic non-bonded pairwise potential is the Lennard-Jones potential[44] that has repulsive and attractive terms that vary as r^{-12} and r^{-6}, respectively, where r is the internuclear separation. Recently, several ion models have augmented this “12-6” potential with an additional r^{-4} term, giving rise to a “12-6-4” potential that provides some improvement[16]. Finally, another potentially useful approach for accounting for electronic polarization in non-polarizable models is to scale partial charges by the inverse of the square root of the dielectric constant of the medium[45–47]. Although no such models exist to date for magnesium ions, parameters for calcium[48] and monovalents like lithium[49] and potassium[50] have been developed.

The ultimate goal of this work is to develop Mg^{2+} ion models that provide a predictive understanding of the ion atmosphere around RNA that is integral to folding. The strategy that we take here is to first identify, or develop if necessary, a Mg^{2+} model that is consistent with the RNA simulation force fields that closely reproduces a range of properties in aqueous solution. The second step, which is forthcoming, involves balancing the Mg^{2+}-water and Mg^{2+}-RNA interactions by tuning pairwise parameters for interactions at particular sites in RNA[3].

In the present work, we explore the accuracy of a broad array of non-bonded single-site Mg^{2+} ion models in molecular simulations. The main goal is to provide insight into the degree to which these ion models are able to simultaneously reproduce structural, thermodynamic, kinetic and mass transport properties in aqueous solution. To our knowledge, there has been no reported study to date that examines all of the Mg^{2+} ion properties considered here, or that compares this wide range of Mg^{2+} ion models together in one place with a consistent set of benchmark quality calculations (including error bars). None of the 17 models examined was able to exactly reproduce the experimental radial distribution function, solvation free energy, exchange barrier and diffusion constant, although the models based on a 12-6-4 potential (which have an additional parameter) offered improvement, and one model in particular, in conjunction with the SPC/E water model performed exceptionally well for all properties. The results reported here characterize the relative strengths and weaknesses of each model, and provide insight into the origin of their behavior that may aid in the development of next-generation models.

Methods

All simulations have been carried out using the AMBER14[17] simulation package and either the SPC/E[51], TIP3P[52] or TIP4PEw[53] water models.

Pairwise potential functional forms

In what follows, electrostatic interactions involving different ion models considered are simple Coulomb pair potentials, $\frac{q_i q_j}{r_{ij}}$, where q_i and q_j are charges located on particles i and j, and r_{ij} is the distance between the particles. Since solvent is modeled explicitly, the dielectric constant in the Coulomb expression is unity. The only difference between the ion models is in the functional form of the non-electrostatic pairwise potential and the parameters that adjust the interactions. These are described below.

The Lennard-Jones (12-6) potential[44] for non-bonded interactions is:

$$U_{ij}(r_{ij}) = \epsilon_{ij}\left[\left(\frac{R_{ij}}{r_{ij}}\right)^{12} - 2\left(\frac{R_{ij}}{r_{ij}}\right)^{6}\right] \quad (1)$$

where the parameters R_{ij} and ε_{ij} are the combined radius and well depth for the pairwise interaction and r_{ij} is the distance between the particles. Eq. 1 can be expressed equivalently as:

$$U_{ij}(r_{ij}) = \frac{A_{ij}}{r_{ij}^{12}} - \frac{B_{ij}}{r_{ij}^{6}} \quad (2)$$

where $A_{ij}=\epsilon_{ij}R_{ij}^{12}$ and $B_{ij}=2\epsilon_{ij}R_{ij}^{6}$.

The standard (12-6) potential can be augmented by an additional r^{-4} term to form a (12-6-4) potential[16] as:

$$U_{ij}(r_{ij}) = \epsilon_{ij}\left[\left(\frac{R_{ij}}{r_{ij}}\right)^{12} - 2\left(\frac{R_{ij}}{r_{ij}}\right)^{6} - 2\kappa R_{ij}^2\left(\frac{R_{ij}}{r_{ij}}\right)^{4}\right] = \frac{A_{ij}}{r_{ij}^{12}} - B_{ij}\left(\frac{1}{r_{ij}^{6}} + \frac{\kappa}{r_{ij}^{4}}\right) \quad (3)$$

where κ is a scaling parameter with units of $Å^{-2}$. The difference between this potential and the 12-6 potential is the additional attractive term, $\kappa\frac{B_{ij}}{r_{ij}^4}$, which falls off as r^{-4} and mimics the charge-induced dipole interaction.

Existing Mg^{2+} models

Table 1 summarizes the Mg^{2+} ion models that will be considered in this study. The Lennard Jones (LJ) parameters for these Mg^{2+} models are characterized by a large radius (1.2-1.6 Å) and a very shallow well depth (0.0013-0.0266 kcal/mol), with the exception of the Åqvist model whose r (0.7926 Å) and ε (0.8947 kcal/mol) are comparatively small and large, respectively. The Åqvist model was originally parametrized with the SPC water model and the constrained spherical boundary model was used to treat the boundary as opposed to periodic boundary conditions[54].

The Mayaan *et al.*, Roux, Allnér *et al.* and Babu & Lim models were all parametrized using the modified TIP3P water model[55] (mTIP3P) which includes vdW radii on the hydrogens and is typically used in the CHARMM molecular dynamics package[56]. The Mayaan *et al.* model[57] aimed to get the correct structure and energetics of Mg^{2+} binding to phosphates relative to water. The Roux model (results unpublished) is the Mg^{2+} ion parameter set found in CHARMM and targets the absolute solvation free energy of Mg^{2+}, as referenced in the CHARMM parameter le for water and ions. Babu & Lim developed parameters by matching the experimental relative solvation free energy between Cd^{2+} and Mg^{2+} [14]. The Allnér *et al.* model is the only parameter set which was parametrized against the experimental Mg^{2+}-water exchange rate.

More recently, a series of water model specific Mg^{2+} parameters have been developed[15,16] and incorporated into AMBER for periodic boundary conditions using PME simulations. These new models include both 12-6 and 12-6-4 parameter sets. The 12-6-4 models target solvation free energy, Mg^{2+}-O equilibrium distance and coordination number while their 12-6 counterparts typically only focus on one of these properties at a time.

Calculation of physical properties

Structure—Normalized radial distribution functions (RDFs), $g_{xy}(r)$,[58] give the probability of two particles (x and y) interacting at a specific distance (r) in solution relative to an ideal gas. Henceforth, we will focus on the distribution of water oxygens around the divalent ion, and designate the RDF simply as $g(r)$. The peaks in the Mg^{2+}-O $g(r)$ show the positions of the solvation shells around the ion, and the coordination numbers for the *ith* solvation shell are obtained by integrating $g(r)$ as follows:

$$CN_i = 4\pi\rho \int_{r_{i-1}^{min}}^{r_i^{min}} g(r)\, r^2 dr; \quad r_0^{min} = 0 \quad (4)$$

where ρ is the bulk particle density of the system and r_1^{min}, r_2^{min} are the locations of the first and second minima in the RDFs, and r_0^{min} is defined as zero.

Thermodynamics—Desolvation free energies for Mg^{2+} are computed using thermodynamic integration (TI) in two steps for the 12-6 models - first the charge is removed, then the vdW parameters. For the 12-6-4 models, an additional step to remove the charge-induced dipole contribution to the energy is included before removing charge.

For both the polarization and charge removing steps, the free energy difference between two states that have potential energies V_0 and V_1 and are linearly coupled is defined as[59]:

$$\Delta G_{TI} = \int_0^1 \left\langle \frac{dV(\lambda)}{d\lambda} \right\rangle_\lambda d\lambda; \quad V(\lambda) = \lambda V_0 + (1-\lambda) V_1 \quad (5)$$

where λ is an order parameter that goes from 0 to 1, and 0 corresponds to the initial state and 1 corresponds to the end state. By running simulations at different λ values one can obtain the quantity $\left\langle \frac{dV(\lambda)}{d\lambda} \right\rangle_\lambda$ directly and the integral in Eq. 5 can be evaluated numerically.

In the final step, the Mg^{2+} ion is decoupled from its environment completely and the form of the so called “softcore” potential is[60]:

$$V_{\text{softcore}} = 4\epsilon(1-\lambda)\left[\frac{1}{\left[0.5\lambda + \left(\frac{r_{ij}}{\sigma}\right)^6\right]^2} - \frac{1}{0.5\lambda + \left(\frac{r_{ij}}{\sigma}\right)^6}\right] \quad (6)$$

where r_{ij} is the distance between the disappearing Mg^{2+} ion and the rest of the system and σ, which is equal to $\frac{R_{ij}}{2^{1/6}}$, is the contact distance at which the potential between the Mg^{2+} 2 ion and the other particles in the system vanishes.

Kinetics—Transition state (TS) theory relates the rate constant (k) and the free energy of activation ($\Delta G^{\dagger}$) as:

$$k = Ae^{-\Delta G^{\dagger}/RT} \quad (7)$$

The pre-exponential factor, A, is in part a measure of the frequency of oscillation for a system about its minima and, for classical TS theory, is estimated to be equal to $k_B T/h$. Computationally, the prefactor can be estimated from the second derivative of the energy at the minimum (E'') of a potential of mean force (PMF) profile, $A = \frac{1}{2\pi}\sqrt{\frac{E''}{\mu}}$ where μ in the reduced mass of Mg^{2+}-O atom pair. The exponential term is a measure of the probability that these oscillations have of crossing the barrier corresponding to an energy of $\Delta G^{\dagger}$.

We have applied transition state theory to estimate water exchange rates for the Mg^{2+} ion models from free energy profiles generated with umbrella sampling simulations along the Mg^{2+}-O distance as a water exchange coordinate.

We employed the vFEP[61,62] method to calculate the free energy profiles from the simulation data and Jacobian corrections were applied. vFEP uses the maximum likelihood principle to determine a robust variational estimate for the free energy profile that is a global analytic function. vFEP does not require a high degree of overlap between umbrella windows and has been shown in many cases to have advantages over other methods such as MBAR[63] and WHAM[64].

Translational diffusion—The diffusion coefficient (*D*) is related to the mean squared displacement (*MSD*) through the Einstein relation[65]:

$$D = \lim_{\to\infty} \frac{1}{6\tau} \left\langle \left| \mathbf{r}\left(t+\tau\right) - \mathbf{r}\left(t\right) \right|^2 \right\rangle \quad (8)$$

where *t* is the simulation time used in the average, τ is the time lag, *D* is the diffusion coefficient and **r** is the position vector of the diffusing particle.

It has been previously shown that diffusion coefficients determined from simulations for water, metal ions, LJ liquids and polymer chains are influenced by nite size effects under periodic boundary conditions[66–70]. A linear relationship between the inverse length of the simulation box and the computed diffusion coefficient can be used to extrapolate the diffusion coefficient (D_o) in the in nite dilution limit:

$$D_o = D_{PBC} + \frac{2.837297 k_B T}{6\pi\eta L} \quad (9)$$

where D_o represents the diffusion coefficient at in nite dilution. D_{PBC} is the calculated diffusion coefficient for each box size, k_B is Boltzmann's constant, T is the temperature in K and η is the solvent viscosity. D_o can be calculated from the y-intercept of the D_{PBC} versus 1/*L* plot, and the viscosity, η, can be determined from the corresponding slope. We will investigate the box size dependence of the diffusion coefficient for the SPC/E, TIP3P and TIP4PEw water models and all 17 Mg^{2+} models using four box sizes.

Simulation protocols

All simulations were carried out using the AMBER14[17] molecular dynamics package. A 9 Å cutoff was applied to non-bonded interactions and the Particle Mesh Ewald (PME)[71] method was employed for the treatment of long range electrostatic interactions. Four box sizes were used in this study (541, 1029, 2311, 4395 total molecules), with box lengths of about 25, 31, 41, 51 A, respectively. The equations of motion were integrated with a 1 fs time step and the target system temperature was set to 298K. All covalent bonds involving hydrogen atoms were constrained with the SHAKE algorithm[72].

Solvation free energies and exchange barriers were computed from NPT simulations while radial distribution functions and diffusion coefficients were obtained from NVT and

NVT/NVE simulations, respectively. For the NPT simulations, the Berendsen barostat[73] was used to keep the pressure constant at 1 atm with a pressure relaxation time of 1 ps and the temperature was maintained by using the Langevin[74] thermostat with a collision frequency of 1 ps^{-1}. For the NVT simulations, the Berendsen thermostat was used instead with a coupling constant of 1 ps (unless otherwise noted in the text). For both NVT and NVE simulations, a more conservative SHAKE tolerance of 10^{-7} Å was enforced (compared to the default SHAKE tolerance in AMBER of 10^{-5} Å).

Ab initio calculations—A high level quantum mechanical (QM) binding energy scan of the Mg^{2+}-oxygen distance of a Mg^{2+} ion and one water molecule (with rigid TIP3P water geometry) was conducted at the counterpoise corrected MP2 level of theory along with the 6-31++G(d,p) basis set using the Gaussian 09 software package[75]. Rigid gas phase binding energy scans for all the Mg^{2+} models, paired with their respective water model, were also performed in AMBER. For all scans, a 0.1 Å ion-oxygen separation distance interval was used.

Radial distribution functions from simulation—Mg^{2+}-O radial distribution functions were calculated using data from 5.0 ns NVT simulations and with the *g*(*r*) GUI plugin in VMD[76] with a bin spacing of 0.05 Å. RDFs were then further re ned by tting a cubic spline to the data points.

Thermodynamic integration simulations—A total of three independent thermodynamic integration simulations[77] were performed for each set Mg^{2+} parameters and average desolvation free energies and standard deviations were obtained. λ values ranged from 0 to 1 and were evenly spaced at 0.1 intervals for all steps. All λ windows were equilibrated for 100 ps with the isothermal-isobaric ensemble, followed by 1 ns NPT production which was used for analysis.

Umbrella sampling simulations—Umbrella sampling simulations for determination of water exchange barriers were started from a 1 ns NPT equilibrated system of Mg^{2+} and water, where the reaction coordinate was chosen as the distance between the Mg^{2+} ion and an inner sphere water oxygen. Stepwise equilibration for 20 ps was conducted for each umbrella window followed by 10 ns NPT production, of which the last 8 ns was ultimately used for analysis. Umbrella windows were positioned at 0.1 Å intervals from 1.6-6.0 Å. In addition, for the 12-6 potential models, whose PMF profiles were characterized by narrower peaks, windows were added around the transition state (0.05 Å intervals) to enhance sampling.

Diffusion simulations—Ideally, diffusion coefficients should be computed from constant energy simulations which follow classical Newtownian dynamics. One technical drawback of NVE simulations, however, is that the average temperature of the simulation may not always be the desired target temperature (Figure S3). Further, depending on the integration time step, integration algorithm and specific software implementation, NVE simulations may be prone to total energy drift over long time scales, which can affect values of dynamical properties[78–80]. A recent study[81] has shown that for NVT simulations velocity randomizing thermostats, such as Langevin[74] and Andersen[82], signi cantly dampen the

dynamics of the system when a small coupling constant is used while velocity rescaling thermostats such as Berendsen[73] and Nosé-Hoover[83–85] closely reproduce constant energy simulation results. It should also be noted that use of the Berendsen thermostat does not properly sample the Maxwell-Boltzmann distribution of kinetic energies[86]. Details on how different thermostats, thermostat coupling schemes and ensembles affect water and Mg^{2+} diffusion results can be found in Supporting Information. The computed diffusion coefficients (Table S3) and temperature distributions (Figure S2) for simulations in the NVE ensemble are very close to the NVT results, thus, we chose to run our diffusion simulations using the NVT ensemble.

All simulations were equilibrated for 1 ns in the NPT ensemble at which point the box size was fixed to the average volume obtained from the second half of the equilibration. Next, 5 ns of NVT equilibration was conducted followed by 21 ns of NVT production, the last 20 ns of which was used for analysis. The length of our diffusion simulations is 20 times longer than typical studies for Mg^{2+} diffusion in the literature[67,87].

Final box size dependent diffusion coefficients (D_{PBC}) were obtained in the following manner: 1) Each simulation is split into 20 1 ns segments 2) $MSD(\tau)$ vs τ plots are generated for each of the 20 1 ns segments where $MSD(\tau)$ is averaged over all molecules at 1 ps time lag intervals out to τ = 100 ps 3) D_{PBC} values are computed using the slope of the $< MSD >$ vs τ plot in the interval $20 \leq \tau \geq 80$ ps and subsequently averaged to yield the reported D_{PBC} values and standard deviations. For the Mg^{2+} models, 20 separate simulations of a single Mg^{2+} ion in aqueous solution were performed for each box size and included in the calculation of D_{PBC}.

Diffusion coefficients at in nite dilution, and corresponding errors, were determined as the y-intercept of the size dependent data through linear regression by generating 1,000 data sets randomly extracted from the normal distribution of the box dependent values and obtaining the corresponding averages and standard deviations. The computed self-diffusion coefficients of Mg^{2+} at in nite dilution $\left(D_0^{sim}\right)$ were further scaled by a factor, $\frac{D_o^w}{\tilde{D}_o^w}$, where D_o^w and $\tilde{D}_o^w$ are the experimental and calculated water diffusion coefficients (Table S4), in order to correct for diffusion errors in the water models and make a more meaningful comparison with experiment.

Results and Discussion

We present the results of a series of MD simulations comparing structural, thermodynamic, kinetic and mass transport properties of Mg^{2+} ion models commonly used in biomolecular simulations. For each property, the Mg^{2+} models are grouped by their respective water models (SPC/E, TIP3P, TIP4PEw), with the exception of the Åqvist model which was originally parametrized in SPC water but is included with the SPC/E Mg^{2+} models in our study. It should also be noted that for all the ion models in the TIP3P water model group, the standard TIP3P water model available in AMBER is utilized for the calculations herein regardless of whether the ion model was originally parametrized with the mTIP3P water model (vdW radii on hydrogens) instead (Table 1). Tables S6-9 suggest that there is a

negligible water model-dependent effect between mTIP3P and TIP3P on the ion model properties studies here.

Reference gas-phase Mg^{2+}-water binding energy scans

The gas phase energetics of a Mg^{2+} ion with a single water molecule are of limited direct relevance to properties in aqueous solution. Nonetheless, analysis of the gas phase energy profiles yields simple properties such as zero energy (contact) distances, minimum energy distances and adiabatic binding energies that are correlated to certain bulk properties and help to facilitate later discussion. Rigid gas phase binding energy scans were obtained for Mg^{2+}-water dimers at 0.1 Å ion-oxygen separation distances in AMBER (Figure 1).

In addition, a high level quantum mechanical (QM) binding energy scan (with rigid TIP3P water geometry) was conducted. Key features of the gas-phase Mg^{2+}-water interaction energy scans are listed in Table 2.

The quantum mechanical reference value for the minimum energy of a Mg^{2+}-water dimer (-79.2 kcal/mol) is generally more negative than the corresponding Mg^{2+} model-water model values with one exception, the TIP4PEw Li *et al.* ΔG_{solv} model. At the same time, the minimum energy distance from the *ab initio* calculation (1.94 Å) is signi cantly larger than that obtained for the Li *et al.* ΔG_{solv} parameter set which has a similar minimum energy. These differences arise primarily from limitations in the static charge force fields which don't explicitly include polarization effects, and therefore do not respond sufficiently to the highly polarizing environment of a coordinated Mg^{2+} ion.

Comparison of the Åqvist and Roux models, which are the default models in AMBER and CHARMM, respectively, indicates that the adiabatic binding energies at -71.1 and -70.8 kcal/mol and minimum energy distances at 1.89 and 1.85 Å are very similar. The strongest interaction energy within each water model category, however, belongs to the Li *et al.* ΔG_{solv} parameter sets which were parametrized against the experimental solvation free energy of Mg^{2+}. These three models also have the smallest Mg^{2+}-O minimum energy distances. Further, going from SPC/E and TIP3P to TIP4PEw, the gas phase binding energy becomes stronger by about 7 kcal/mol. When comparing the 12-6-4 models, we see that the minimum energy ranges between -66.5 kcal/mol (SPC/E) to about -65 kcal/mol (TIP3P/TIP4PEw), which for all water models, is less than the corresponding Li *et al.* ΔG_{solv} parameter sets. Contact distances (σ) are also correlated with minimum energy distances; the larger R, the larger σ.

A general correlation is observed between the binding energy in the gas phase and the solvation free energy of the 12-6 models (see Thermodynamics: solvation free energy values section). A linear correlation also exists between the minimum energies distances from the adiabatic scans and the locations of the first solvation shell peaks in the RDFs (see Structure: Mg^{2+}-water oxygen radial distribution functions section).

Structure: Mg^{2+}-water oxygen radial distribution functions

Various X-ray diffraction[88–92], NMR[93,94], and IR and Raman spectroscopic[95] studies have shown that Mg^{2+} ions are hexacoordinated by water ligands in an octahedral geometry in

aqueous solution. A first shell Mg^{2+}-O distance of 2.09 ± 0.04 Å, which is averaged over all available diffraction data collected in a comprehensive review by Marcus[96], and a second shell range of 4.1-4.2 Å, also based on accumulated diffraction experiments in a review by Ohtaki & Radnai[97], will be used as the reference values for all model comparisons.

The Mg^{2+}-O RDFs are illustrated for the 17 Mg^{2+} models in Figure 2 and key properties are listed in Table 3. The RDFs illustrate the characteristically narrow first shell distribution and the wide, extended distribution of the second solvation shell. For all models, the second solvation shell peaks are very similar in shape and location. The main differences between the RDFs can be found in the first solvation shell, where the positions of the peaks are shifted relative to each other. For the TIP4PEw Mg^{2+} models, the shapes of the first peak in the RDF vary as well. The maximum $g(r)$ in the first solvation shell is between 20-25 for all models except for the TIP4PEw Li *et al.* ΔG_{solv} model, which has a maximum $g(r)$ closer to 15 (Table 3).

Table 3 summarizes the positions of the first and second solvation shell maxima and minima distances and the average coordination numbers for these shells. For the first solvation shell, peak distances range from 1.89-2.11 Å among the models while for the second solvation shell peak distances range from 4.09-4.37 Å. A general trend observed is that the closer the first solvation shell is to Mg^{2+}, the closer is the second shell. The Li *et al.* ΔG_{solv} parameters have the tightest first solvation shells within their water model groups and do not fall within experimental error. In fact, the only models that do match this property within experimental error are those which have been parametrized against it. That is, the Mayaan *et al.*, Babu & Lim, and all the Li *et al.* $R_{Mg^{2+}\text{-}O}$ models from the 12-6 model category along with all the 12-6-4 models. The coordination numbers for the first and second solvation shells, CN_1 and CN_2, were also calculated. The CN_1 value is found to be 6 for all models and agrees with the experimental first coordination number. The calculated CN_2 values, on the other hand, are more variable, ranging from about 13-17. These values are consistently larger than the experimental value of 12. The TIP3P Mg^{2+} models tend to have the largest CN_2 values compared with both the SPC/E and TIP4PEw Mg^{2+} models.

Thermodynamics: solvation free energy values

Experimentally, the standard hydration free energies of ions are typically measured relative to H^+. Therefore, the absolute hydration free energy of H^+ is required to estimate the absolute hydration free energy of Mg^{2+}, which can vary according to different sources. One approach, that of Marcus, uses proton hydration free energies from the National Bureau of Standards compilation and has been heavily used as a reference in Mg^{2+} model development[14–16,98]. Thus, in the present study, the reference standard solvation free energy of Mg^{2+} (-437.4 kcal/mol) follows Marcus's approach where

$\Delta G^{\circ}_{solv}\quad H^{+} = -1056\quad kJ/mol$[99].

Figure 3a summarizes absolute solvation free energies computed for the Mg^{2+} models tested in this study. When computing the solvation free energy using both the SPC/E and the SPC water models for the Åqvist parameter set we see a difference of more than 20 kcal/mol compared to the published value of -455.5 kcal/mol[54]. This is an extreme example of how

differences in simulation protocol can affect calculated solvation free energies. Li *et al.* have recently also tried to reproduce the solvation free energy using the Åqvist parameters and see the same discrepancy[15]. See Table S1 for more information on comparison of computed solvation free energies with published values.

As for the rest of the models, all those that targeted properties other than absolute solvation free energy, including phosphate binding (Mayaan *et al.*), equilibrium Mg^{2+}-O distance or coordination number (Li *et al.* models), water exchange barrier (Allnér *et al.*), and relative solvation free energy (Babu & Lim) grossly underestimate the experimental solvation free energy of -437.4 kcal/mol[99] by about 25 (SPC/E Li *et al.* CN set) to 55 (TIP4PEw Li *et al.* $R_{Mg^{2+}\text{-}O}$ set) kcal/mol. This is a consequence of the static charge force field which uses prepolarized waters with increased permanent dipole moments compared to the gas phase (1.855 D); however, this degree of implicit polarization is optimized for a bulk water environment, rather than in the inner sphere of a divalent ion.

Figure 3b illustrates the behavior of fixed charge Mg^{2+} models in terms of their inability to reproduce both structural and thermodynamic experimental observables and highlights the importance of including polarization effects to this regard. The computed solvation free energies are correlated with the inverse first shell Mg^{2+}-O distances; the closer a given parameter gets to the experimental Mg^{2+}-O distance, the more under solvated it becomes. TIP4PEw Mg^{2+} models are more undersolvated than SPC/E and TIP3P models at the same Mg^{2+}-O distances. The models which include the induced dipole interaction (*i.e.* the 12-6-4 models)[16], on the other hand, come very close to reproducing both the experimental hydration free energy and equilibrium Mg^{2+}-O distance with our simulation protocol. It should be noted that free energy simulations with non-polarizable point charge models, in some cases, may reproduce experimental solvation free energies as a result of a cancellation of errors (e.g., lack of electronic polarization counterbalanced by incorrect bare solute charges)[45].

Kinetics: Mg^{2+}-water exchange rates

Water exchange rates for diamagnetic metal ions can in principle be directly obtained from ^{17}O NMR relaxation experiments. For Mg^{2+}, however, whose first shell waters exchange relatively fast ($> 10^4$ s^{-1}), a ^{17}O NMR bound water resonance is not visible on the NMR spectrum unless addition of either a paramagnetic chemical shift agent or a paramagnetic relaxation agent is employed. There have been two such studies[100,101] which have obtained water exchange rates for Mg^{2+}, $5.3 \pm 0.3 \times 10^5$ s^{-1} and $6.7 \pm 0.2 \times 10^5$ s^{-1}, the latter of which is used as the reference for this study because the experiment was carried out in 0.18 mol/kg salt concentration versus a 3.52 mol/kg salt concentration in the former study.

To date, there has been relatively little consideration of exchange rates in the development of Mg^{2+} ion models[98]. On the time scales accessible to conventional molecular simulations, the Mg^{2+}-water exchange rates are not easily observed directly. Consequently, an alternative method to determine the exchange rate is to compute the free energy profile along an exchange coordinate and use transition state theory to estimate the rate. We have obtained free energy barriers and rates for water exchange in the first solvation shell from potential of

mean force profiles (Figure 4). These free energy profiles show a spread in barrier heights, barrier peak shapes and transition state locations across water model groups (Table 4).

The position of the transition state ($R^{\dagger}$) is correlated with the $R_{Mg^{2+}\text{-}O}$ distance for the 12-6 models; the smaller $R_{Mg^{2+}\text{-}O}$, the larger $R^{\dagger}$. The 12-6-4 models have $R^{\dagger}$ values around 2.65 Å. About half the models yield barriers that are too high compared with experiment, while the other half yield barriers that are either close to experiment or too low. Interestingly, the models with the highest barrier heights in the SPC/E and TIP3P groups are the Åqvist and Roux models with barriers of 13.9 and 12.9 kcal/mol, respectively. This corresponds to rates that are three and two orders of magnitude lower than the experimental value of 6.7 ± 10^5 s^{-1}[101]. Allnér *et al.* also computed the barrier to exchange for the Roux model with mTIP3P waters and obtained 12.7 ± 0.2 kcal/mol. For the Allnér *et al.* model itself, however, we calculate a barrier of 10.9 ± 0.1 which is 1 kcal/mol higher than the previously published value[98] using a slightly different simulation protocol. Among the Li *et al.* models there is also a clear trend across water models - the barriers of the ΔG_{solv}, $R_{Mg^{2+}\text{-}O}$ and CN sets decrease from SPC/E to TIP3P to TIP4PEw. With the 12-6-4 models, it is interesting to see that although enhanced implicit polarization effects are included in the models and their thermodynamic and structural properties match well with experiment, they do not all have good kinetic behavior. The TIP3P and TIP4PEw 12-6-4 models overestimate the rate of exchange by an order of magnitude. The SPC/E 12-6-4 model, on the other hand, is the only one that is within error of the experimental $log(k_1)$, and performs best with this property compared with the other 16 models in our study even though it was not parametrized to get this property correct. It is also important to note that the Allnér *et al.* model, which was originally tted to the experimental exchange rate, is the only other model that we observe to have kinetics on the same order of magnitude as in experiment.

Mass transport properties: Mg^{2+} diffusion coefficients and viscosities

To our knowledge, the only experimental translational diffusion coefficient at in nite dilution available for Mg^{2+} (as obtained from tracer diffusion experiments of ^{28}Mg in $MgCl_2$ solutions) is 0.706×10^{-5} cm^2/s[102] and this value will be used as a reference to compare with computed diffusion coefficients. The experimental viscosity of water[103], 8.903×10^{-4} $kgm^{-1}s^{-1}$, will also be compared with our calculated solvent viscosities.

Despite its importance as a fundamental bulk transport property, diffusion coefficients are often neglected in the parametrization of Mg^{2+} ion models. Accurate calculation of the diffusion coefficient at in nite dilution requires consideration of the size of the simulation cell, as well as consideration of systematic errors in the diffusion of modeled water molecules. Figure 5 illustrates the dependence of the calculated diffusion coefficients on the box size for four Mg^{2+}-water systems consisting of 1 Mg^{2+} ion and either 540, 1028, 2310 or 4394 water molecules.

In order to directly compare Mg^{2+} diffusion coefficients $\left(D_o^{sim}\right)$ with experiment in the dilute limit using different water models, they must be re-scaled (D_o) to correct for systematic errors in the diffusion coefficients of the water models themselves (see discussion in Methods section). Table 5 lists the scaled values of the simulated diffusion

coefficients, viscosities and hydrodynamic radii at in nite dilution that will be referred to for the remainder of this discussion (Table S5 lists the corresponding unscaled values for reference).

Overall, the calculated values for the scaled in nite dilution diffusion coefficients ranged between 0.723 and 0.813 × 10^{-5}cm^2/s, slightly higher than the experimental value of 0.706 × 10^{-5}cm^2/s. No obvious trend is evident from the diffusion results (Table 5), although it should be pointed out that the standard deviations for individual diffusion coefficient values are fairly large relative to the differences between average values making any conclusion about average trends likely not statistically signi cant. Individual diffusion coefficients for the SPC/E Mg^{2+} models are most similar while the TIP4PEw Mg^{2+} models show the most variation for a given box size. Although none of the Mg^{2+} SPC/E models were originally parametrized to match translation diffusion, their computed scaled D_o values are all within error of the experimental translational diffusion coefficient. The same can be said for two of the TIP4PEw Mg^{2+} models, the Li *et al.* ΔG_{solv} and CN sets. All the TIP3P Mg^{2+} models, on the other hand, have scaled diffusion coefficients that are slightly too high (e.g., beyond the simulated standard deviations).

Solvent viscosities can be extracted from the slopes of the (scaled) D_{PBC} versus 1/L plot as previously discussed and these are summarized in Table 5. The Roux model, which has the largest scaled diffusion coefficient, has the smallest scaled solvent viscosity among all the models, 7.64 × 10^{-4} kgm^{-1}s^{-1}. The SPC/E Li *et al.* CN model is on the other end of the spectrum with the smallest scaled diffusion coefficient and largest scaled solvent viscosity of 9.81 × 10^{-4} kgm^{-1}s^{-1}. It is also interesting to note that although the SPC/E Li *et al.* CN model has the scaled diffusion coefficient that matches experiment best, the corresponding scaled solvent viscosity is too high compared to the experimental value.

By applying the Stokes-Einstein relation[65] we can also estimate the effective hydrodynamic radius of the Mg^{2+} ion models using our computed (scaled) D_o values and solvent viscosities:

$$D=\frac{k_B T}{6\pi\eta r} \quad (10)$$

where k_B is the Boltzmann constant, T is the temperature in K, η is the solvent viscosity and r is the radius of a spherical particle. Comparing the simulated values from Table 5 gives effective hydrodynamic radii in the ranges of 3.07-3.24, 3.02-3.50 and 3.36-3.50 Å for SPC/E, TIP3P and TIP4PEw, respectively.

Conclusion

The importance of Mg^{2+} ions for biomolecular structure, dynamics and function has been a driving force for the development of Mg^{2+} models in recent years.

In an effort to better understand the strengths and weaknesses of an existing set of 17 different Mg^{2+} ion models, we evaluated their ability to simultaneously reproduce structural, thermodynamic, kinetic and mass transport properties in aqueous solution. These represent a

balanced set of solution properties that serve as a useful departure point from which robust models for molecular dynamics simulations of biological processes can be developed by tuning pairwise interaction parameters.

Certain bulk properties such as the first shell Mg^{2+}-O distances and solvation free energies were observed to be correlated to the minimum energy distances and adiabatic binding energies from gas phase binding energy scans. Most of the models considered either overestimate or underestimate the inner shell water exchange barrier by several kcal/mol. On the other hand, mass transport properties were observed to be somewhat insensitive to the models. The simple 12-6 models were shown to have considerable limitations regardless of the water model used or the specific LJ parameters. These models were not able to simultaneously reproduce both structural and thermodynamic properties with reasonable accuracy. The 12-6-4 models, on the other hand, offer respectable improvement, particularly with respect to matching both the radial distribution function and solvation free energy. One model in particular, the SPC/E 12-6-4 model of Li *et al.*, performs extremely well across all properties (within statistical confidence) despite only being originally parametrized to match structure and thermodynamics.

This detailed analysis of the solution properties predicted by several Mg^{2+} models used in molecular simulations provides a baseline from which to gauge progress and direct future effort. In progressing toward improved force field models for simulations of biomolecules, and in particular RNA, under different ionic conditions, it is important to properly balance the ion-water, ion-ion and ion-biomolecule interactions. This underscores the importance of testing the models with respect to binding to protein, DNA and RNA systems, and comparing simulation results against quantitative measurements such as specific binding constants and exchange rates, and results from ion counting experiments (including ion competition).

Supplementary Material

Refer to Web version on PubMed Central for supplementary material.

Acknowledgments

Financial support was provided by the National Institute of Health grant P01GM066275 (D.M.Y.). This work was supported by computational resources including the Blue Waters supercomputer, supported by the National Science Foundation (NSF) grant numbers ACI-0725070 and ACI-1238993, and the Extreme Science and Engineering Discovery Environment (XSEDE), supported by NSF grant number OCI-1053575. We are also thankful for insightful comments from Daniel Herschlag and members of his lab.

References

1. Draper DE. RNA. 2004; 10:335. [PubMed: 14970378]
2. Freisinger E, Sigel RKO. Coordin. Chem. Rev. 2007; 251:1834.
3. Sigel RKO, Sigel H. Acc. Chem. Res. 2010; 43:974. [PubMed: 20235593]
4. Hammann C, Norman DG, Lilley DMJ. Proc. Natl. Acad. Sci. USA. 2001; 98:5503. [PubMed: 11331743]
5. Das R, Travers KJ, Bai Y, Herschlag D. J. Am. Chem. Soc. 2005; 127:8272. [PubMed: 15941246]

6. Laederach A, Shcherbakova I, Jonikas MA, Altman RB, Brenowitz M. Proc. Natl. Acad. Sci. USA. 2007; 104:7045. [PubMed: 17438287]
7. Frederiksen JK, Li N-S, Das R, Herschlag D, Piccirilli JA. RNA. 2012; 18:1123. [PubMed: 22539523]
8. Pyle AM. J. Biol. Inorg. Chem. 2002; 7:679. [PubMed: 12203005]
9. DeRose VJ. Curr. Opin. Struct. Biol. 2003; 13:317. [PubMed: 12831882]
10. Schnabl J, Sigel RKO. Curr. Opin. Chem. Biol. 2010; 14:269. [PubMed: 20047851]
11. Ferré-D'Amaré AR, Scott WG. Cold Spring Harb Perspect Biol. 2010; 2:a003574. [PubMed: 20843979]
12. Ward WL, Plakos K, DeRose VJ. Chem. Rev. 2014; 114:4318. [PubMed: 24730975]
13. Martínez JM, Pappalardo RR, Marcos ES. J. Am. Chem. Soc. 1999; 121:3175.
14. Babu CS, Lim C. J. Phys. Chem. A. 2006; 110:691. [PubMed: 16405342]
15. Li P, Roberts BP, Chakravorty DK, Merz KM Jr. J. Chem. Theory Comput. 2013; 9:2733. [PubMed: 23914143]
16. Li P, Merz KM Jr. J. Chem. Theory Comput. 2014; 10:289. [PubMed: 24659926]
17. Case, D.; Babin, V.; Berryman, J.; Betz, R.; Cai, Q.; Cerutti, D.; Cheatham, T., III; Darden, T.; Duke, R.; Gohlke, H., et al. AMBER 14 (University of California. San Francisco, San Francisco, CA: 2014.
18. Cornell WD, Cieplak P, Bayly CI, Gould IR, Merz KM Jr. Ferguson DM, Spellmeyer DC, Fox T, Caldwell JW, Kollman PA. J. Am. Chem. Soc. 1995; 117:5179.
19. Wang J, Cieplak P, Kollman PA. J. Comput. Chem. 2000; 21:1049.
20. Pérez A, Marchán I, Svozil D, Sponer J, Cheatham TE III, Laughton CA, Orozco M. Biophys. J. 2007; 92:3817. [PubMed: 17351000]
21. Zgarbová M, Otyepka M, Šponer J, Mládek A, Banáš P, Cheatham TE III, Jurečka P. J. Chem. Theory Comput. 2011; 7:2886. [PubMed: 21921995]
22. MacKerell AD Jr. Banavali NK. J. Comput. Chem. 2000; 21:105.
23. Foloppe N, MacKerell AD Jr. J. Comput. Chem. 2000; 21:86.
24. Oostenbrink C, Villa A, Mark AE, van Gunsteren WF. J. Comput. Chem. 2004; 25:1656. [PubMed: 15264259]
25. Jorgensen WL, Maxwell DS, Tirado-Rives J. J. Am. Chem. Soc. 1996; 118:11225.
26. Kaminski GA, Friesner RA, Tirado-Rives J, Jorgensen WL. J. Phys. Chem. B. 2001; 105:6474.
27. Ponder JW, Wu C, Ren P, Pande VS, Chodera JD, Schnieders MJ, Haque I, Mobley DL, Lambrecht DS, DiStasio RA Jr. et al. J. Phys. Chem. B. 2010; 114:2549. [PubMed: 20136072]
28. Jiao D, King C, Gross eld A, Darden TA, Ren P. J. Phys. Chem. B. 2006; 110:18553. [PubMed: 16970483]
29. Grossfield A, Ren P, Ponder JW. J. Am. Chem. Soc. 2003; 125:15671. [PubMed: 14664617]
30. Lamoureux G, Roux B. J. Phys. Chem. B. 2006; 110:3308. [PubMed: 16494345]
31. Piquemal J-P, Perera L, Cisneros GA, Ren P, Pedersen LG, Darden TA. J. Chem. Phys. 2006; 125:054511. [PubMed: 16942230]
32. Yu H, Whitfield TW, Harder E, Lamoureux G, Vorobyov I, Anisimov VM, MacKerell AD Jr. Roux B. J. Chem. Theory Comput. 2010; 6:774. [PubMed: 20300554]
33. Spångberg D, Hermansson K. J. Chem. Phys. 2004; 120:4829. [PubMed: 15267343]
34. Peters MB, Yang Y, Wang B, Füsti-Molnár L, Weaver MN, Merz KM Jr. J. Chem. Theory Comput. 2010; 6:2935. [PubMed: 20856692]
35. Bredenberg J, Nilsson L. Int. J. Quantum Chem. 2001; 83:230.
36. Hoops SC, Anderson KW, Merz KM Jr. J. Am. Chem. Soc. 1991; 113:8262.
37. Stote RH, Karplus M. Proteins. 1995; 23:12. [PubMed: 8539245]
38. Helm L, Merbach AE. Coord. Chem. Rev. 1999; 187:151.
39. Saxena A, Sept D. J. Chem. Theory Comput. 2013; 9:3538.
40. Åqvist J, Warshel A. J. Am. Chem. Soc. 1990; 112:2860.
41. Pang Y-P. J. Mol. Model. 1999; 5:196.

42. Pang Y-P, Xu K, El Yazal J, Prendergast FG. Protein Sci. 2000; 9:1857. [PubMed: 11106157]
43. Oelschlaeger P, Klahn M, Beard WA, Wilson SH, Warshel A. J. Mol. Biol. 2007; 366:687. [PubMed: 17174326]
44. Jones JE. Proc. R. Soc. Lond. A. 1924; 106:463.
45. Leontyev IV, Stuchebrukhov AA. Phys. Chem. Chem. Phys. 2011; 13:2613. [PubMed: 21212894]
46. Leontyev IV, Stuchebrukhov AA. J. Chem. Theory Comput. 2010; 6:1498. [PubMed: 25364313]
47. Leontyev IV, Stuchebrukhov AA. J. Chem. Phys. 2014; 141:014103. [PubMed: 25005273]
48. Kohagen M, Mason PE, Jungwirth P. J. Phys. Chem. B. 2014; 118:7902. [PubMed: 24802184]
49. Pluhařová E, Mason PE, Jungwirth P. J. Phys. Chem. A. 2013; 117:11766. [PubMed: 23581250]
50. Mason PE, Wernersson E, Jungwirth P. J. Phys. Chem. B. 2012; 116:8145. [PubMed: 22630587]
51. Berendsen HJC, Grigera JR, Straatsma TP. J. Phys. Chem. 1987; 91:6269.
52. Jorgensen WL, Chandrasekhar J, Madura JD, Impey RW, Klein ML. J. Chem. Phys. 1983; 79:926.
53. Horn HW, Swope WC, Pitera JW, Madura JD, Dick TJ, Hura GL, Head-Gordon T. J. Chem. Phys. 2004; 120:9665. [PubMed: 15267980]
54. Åqvist J. J. Phys. Chem. 1990; 94:8021.
55. Neria E, Fischer S, Karplus M. J. Chem. Phys. 1996; 105:1902.
56. Brooks BR, Brooks CL III, MacKerell AD Jr. Nilsson L, Petrella RJ, Roux B, Won Y, Archontis G, Bartels C, Boresch S, et al. J. Comput. Chem. 2009; 30:1545. [PubMed: 19444816]
57. Mayaan E, Moser A, MacKerell AD Jr. York DM. J. Comput. Chem. 2007; 28:495. [PubMed: 17186477]
58. Frenkel, D.; Smit, B. Understanding Molecular Simulation. Academic Press; San Diego, CA: 2002.
59. Kirkwood JG. J. Chem. Phys. 1935; 3:300.
60. Steinbrecher T, Joung I, Case DA. J. Comput. Chem. 2011; 32:3253. [PubMed: 21953558]
61. Lee T-S, Radak BK, Pabis A, York DM. J. Chem. Theory Comput. 2013; 9:153. [PubMed: 23457427]
62. Lee T-S, Radak BK, Huang M, Wong K-Y, York DM. J. Chem. Theory Comput. 2014; 10:24. [PubMed: 24505217]
63. Shirts MR, Chodera JD. J. Chem. Phys. 2008; 129:124105. [PubMed: 19045004]
64. Gross eld, A. [April 2012] WHAM: the weighted histogram analysis method [Online], version 2.0.4. http://membrane.urmc.rochester.edu/content/wham
65. Einstein A. Annalen der Physik. 1905; 17:549.
66. Dünweg B, Kremer K. J. Chem. Phys. 1993; 99:6983.
67. Obst S, Bradaczek H. J. Phys. Chem. 1996; 100:15677.
68. Spångberg D, Hermansson K. J. Chem. Phys. 2003; 119:7263.
69. Yeh I-C, Hummer G. J. Phys. Chem. B. 2004; 108:15873.
70. Tazi S, Boţan A, Salanne M, Marry V, Turq P, Rotenberg B. J. Phys. Condens. Matter. 2012; 24:284117. [PubMed: 22739097]
71. Darden T, York D, Pedersen L. J. Chem. Phys. 1993; 98:10089.
72. Ryckaert JP, Ciccotti G, Berendsen HJC. J. Comput. Phys. 1977; 23:327.
73. Berendsen HJC, Postma JPM, van Gunsteren WF, Dinola A, Haak JR. J. Chem. Phys. 1984; 81:3684.
74. Turq P, Lantelme F, Friedman HL. J. Chem. Phys. 1977; 66:3039.
75. Frisch, MJ.; Trucks, GW.; Schlegel, HB.; Scuseria, GE.; Robb, MA.; Cheeseman, JR.; Scalmani, G.; Barone, V.; Mennucci, B.; Petersson, GA., et al. Gaussian09 Revi sion D.01. gaussian Inc.; Wallingford CT: 2009.
76. Humphrey W, Dalke A, Schulten K. J. Mol. Graphics. 1996; 14:33.
77. Kaus JW, Pierce LT, Walker RC, McCammon JA. J. Chem. Theory Comput. 2013; 9:4131.
78. Harvey SC, Tan RKZ, Cheatham III TE. J. Comp. Chem. 1998; 19:726.
79. Cottrell D, Tupper PF. BIT Num. Math. 2007; 47:507.
80. Lamoureux G, Roux B. J. Chem. Phys. 2003; 119:3025.

81. Basconi JE, Shirts MR. J. Chem. Theory Comput. 2013; 9:2887.
82. Andersen HC. J. Chem. Phys. 1980; 72:2384.
83. Nosé S. J. Chem. Phys. 1984; 81:511.
84. Hoover WG. Phys. Rev. A. 1985; 31:1695. [PubMed: 9895674]
85. Martyna GJ, Klein ML, Tuckerman M. J. Chem. Phys. 1992; 97:2635.
86. Shirts MR. J. Chem. Theory Comput. 2013; 9:909.
87. Guàrdia E, Sesé G, Padró JA, Kalko SG. J. Solut. Chem. 1999; 28:1113.
88. Dorosh AK, Skryshevskii AF. J. Struct. Chem. 1964; 5:842.
89. Caminiti R, Licheri G, Piccaluga G, Pinna G. J. Appl. Cryst. 1979; 12:34.
90. Bol W, Gerrits GJA, van Panthaleon van Eck CL. J. Appl. Cryst. 1970; 3:486.
91. Albright JN. J. Chem. Phys. 1972; 56:3783.
92. Caminiti R. Chem. Phys. Lett. 1982; 88:103.
93. Matwiyoff NA, Taube H. J. Am. Chem. Soc. 1968; 90:2796.
94. Vogrin BJ, Knapp PS, Flint WL, Anton A, Highberger G, Malinowski ER. J. Chem. Phys. 1971; 54:178.
95. Lesiecki ML, Nibler JW. J. Chem. Phys. 1976; 64:871.
96. Marcus Y. Chem. Rev. 1988; 88:1475.
97. Ohtaki H, Radnai T. Chem. Rev. 1993; 93:1157.
98. Allnér O, Nilsson L, Villa A. J. Chem. Theory Comput. 2012; 8:1493.
99. Marcus Y. J. Chem. Soc. Faraday Trans. 1991; 87:2995.
100. Neely J, Connick R. J. Am. Chem. Soc. 1970; 92:3476.
101. Bleuzen A, Pittet P-A, Helm L, Merbach AE. Magn. Reson. Chem. 1997; 35:765.
102. Struis RPWJ, de Bleijser J, Leyte JC. J. Phys. Chem. 1987; 91:6309.
103. Korson L, Drost-Hansen W, Millero FJ. J. Phys. Chem. 1969; 73:34.

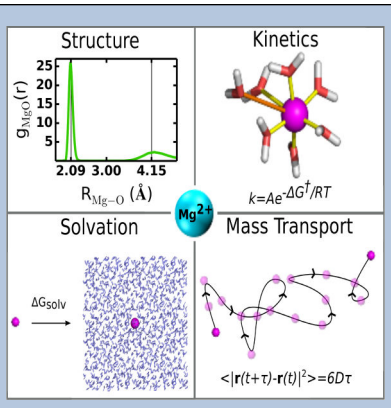

Mg^{2+} ions are essential for nucleic acid structure and function and this has motivated the development of several Mg^{2+} models for use in molecular simulations. As a first step in developing improved Mg^{2+} models for biomolecular simulations, we focus on the ability to which 17 different pairwise potential Mg^{2+} models, which belong to the most mature force fields for modeling nucleic acid dynamics, can simultaneously reproduce structural, thermodynamic, kinetic and mass transport properties in aqueous solution. These represent a balanced set of solution properties that serve as a useful departure point from which robust models for molecular dynamics simulations of biological processes can be developed by tuning pairwise interaction parameters.

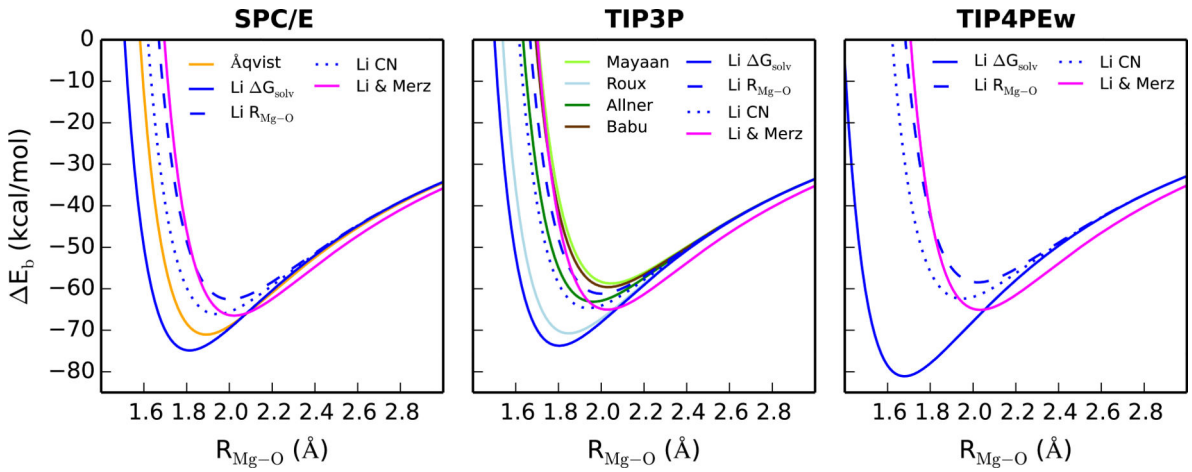

Figure 1.

Total binding energy (ΔE_b) of Mg^{2+} with a single water molecule in the gas phase versus ion-oxygen separation distance ($R_{Mg^{2+}\text{-}O}$) for the Mg^{2+} models and their respective water models.

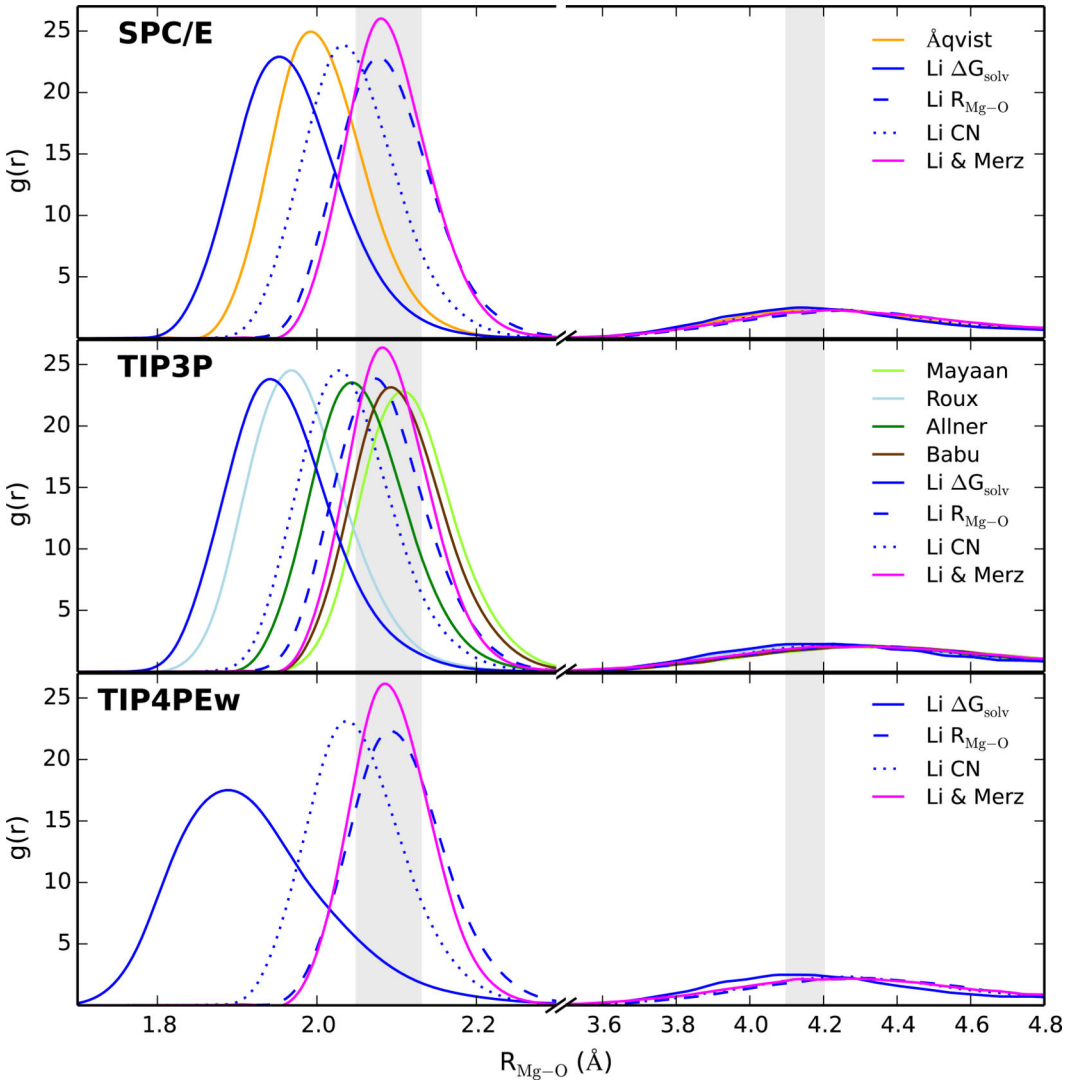

Figure 2.

Normalized radial distribution functions for Mg^{2+} models grouped by water model. Top: SPC/E, Middle: TIP3P, Bottom: TIP4PEw. Gray vertical lines at 2.09 ± 0.04 Å and 4.1-4.2 Å represent the ranges of experimental equilibrium Mg^{2+}-O distances for the first and second solvation shells, respectively.

(a) Absolute Mg^{2+} solvation free energies. Errors bars are on the order of 0.1 kcal/mol.

(b) Relationship between computed solvation free energies and inverse first shell Mg^{2+}-O distances.

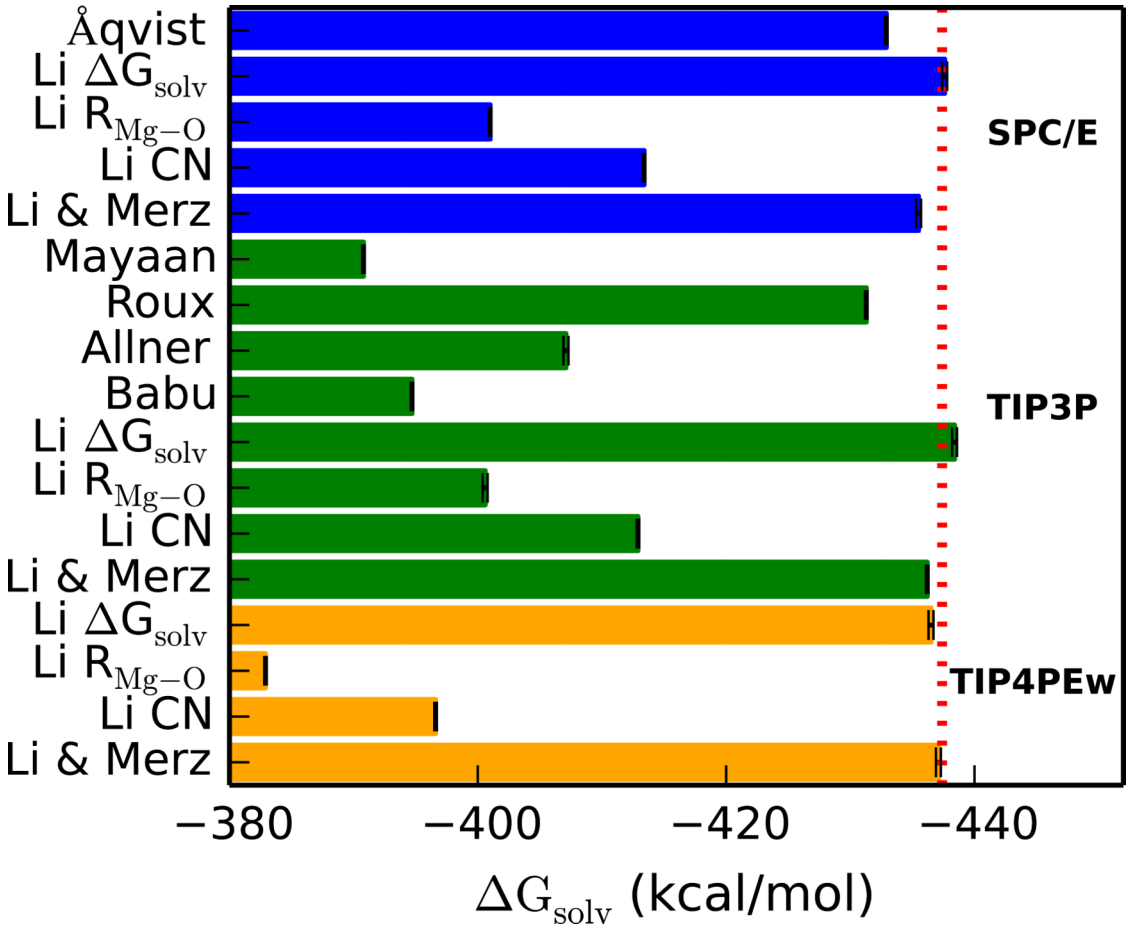

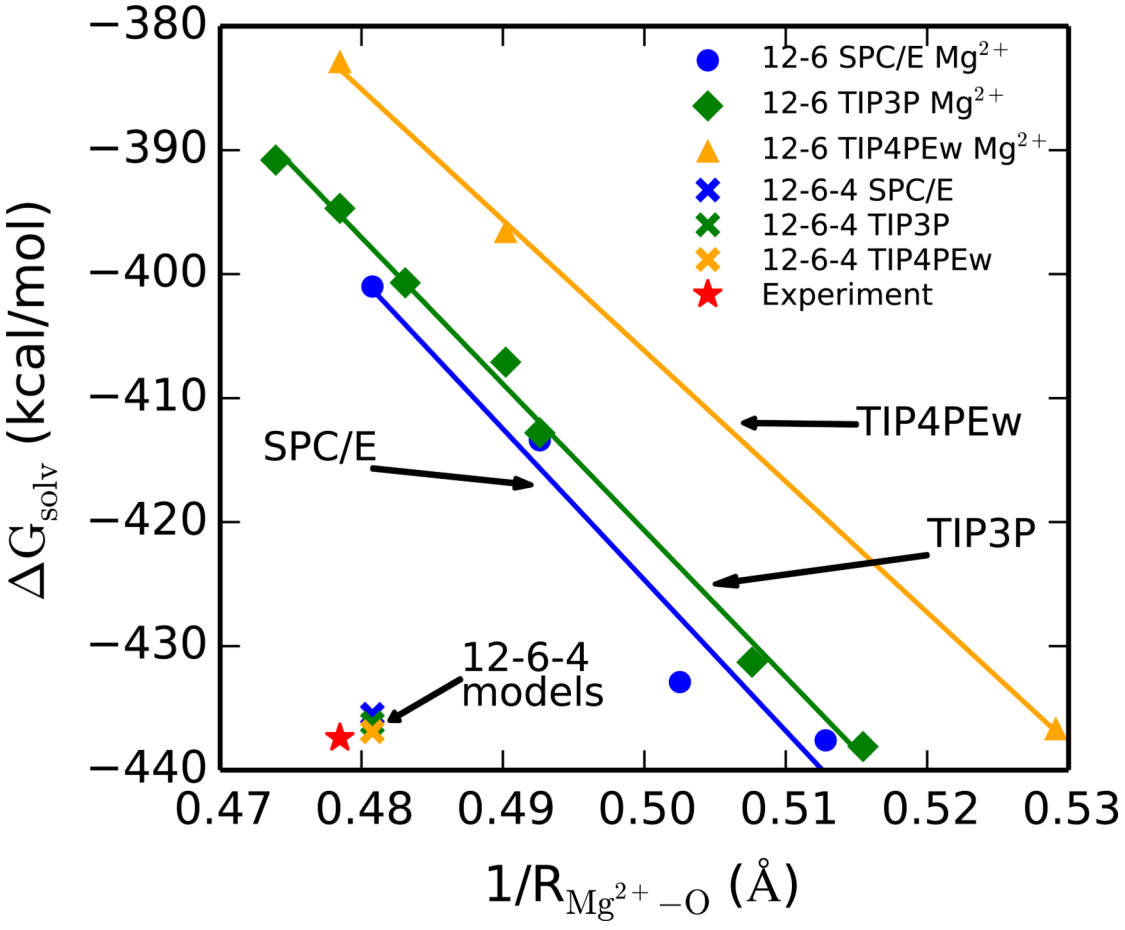

Figure 3.

a) Summary of solvation free energies collected for the Mg^{2+} models compared with experiment (dashed red line) and b) their correlation with inverse equilibrium Mg^{2+}-oxygen distances, both grouped by water model.

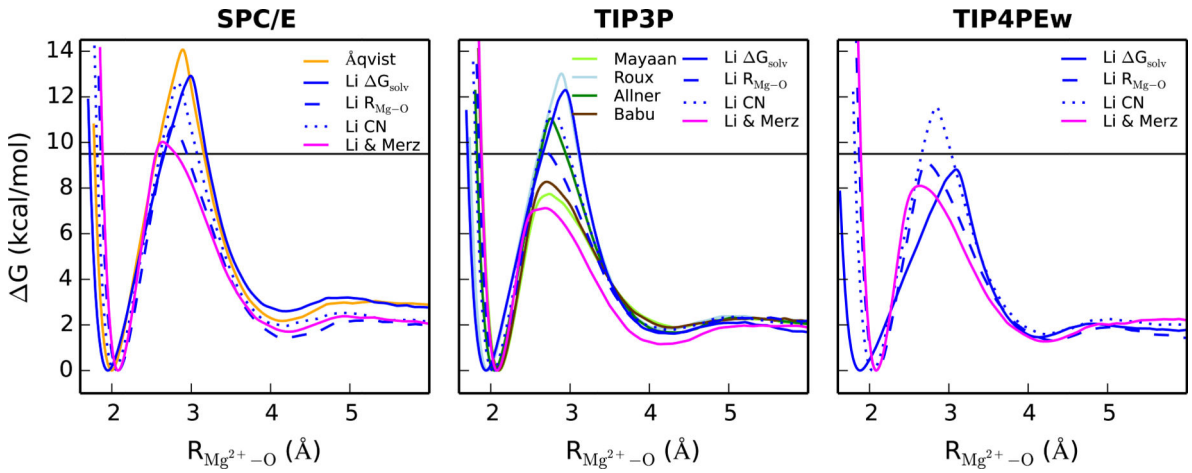

Figure 4.

Potential of mean force between Mg^{2+} and water oxygen grouped by water model and obtained from the last 2 ns of umbrella sampling data. The horizontal solid line at 9.5 kcal/mol represents the reference $\Delta G^{\dagger}$ that corresponds to the experimental water exchange rate of 6.7×10^5 s^{-1} with the pre-exponential factor estimated as k_BT/h.

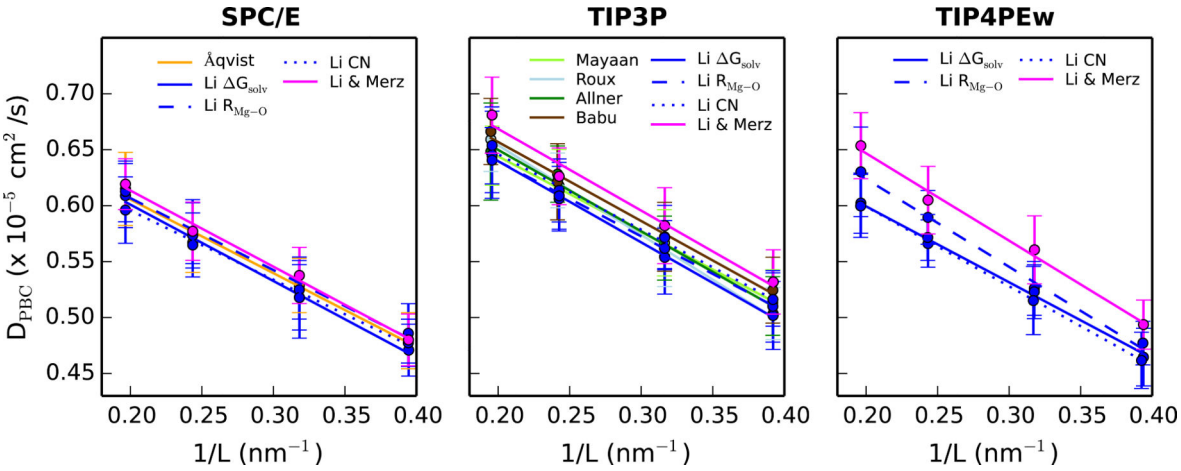

Figure 5.

Dependence of calculated diffusion coefficients for Mg^{2+} models (D_{PBC}) scaled D^w by the ratio of experimental and computed water diffusion coefficients $\left(\frac{D_o^w}{D_o^w}\right)$ to correct for diffusion errors in the water models.

Table 1

Summary of the Mg^{2+} models examined in this study. The parameters R, ε and κ are described in the text. The main properties considered in the parametrization include: $R_{Mg^{2+}\text{-}O}$ (first solvation shell Mg^{2+}-O distance), RDF (radial distribution function), CN (coordination number), ΔG_{solv} (solvation free energy), ΔE (interaction energy) and k_1 (first shell water exchange rate).

Model	R (Å)	ε (cal/mol)	κ (Å^{-2})	Water Model	Properties[a]
Åqvist[54]	0.7926	894.70000	—	SPC	ΔG_{solv}, RDF
Mayaan *et al.*[57]	1.4647	14.00000	—	mTIP3P[b]	structure, ΔE[c]
Roux[d]	1.1850	15.00000	—	mTIP3P	ΔG_{solv}
Allnér *et al.*[98]	1.5545	2.95000	—	mTIP3P	k_1
Babu & Lim[14]	1.3636	26.60000	—	mTIP3P	ΔG_{solv},$R_{Mg^{2+}\text{-}O}$,CN
Li *et al.* (ΔG_{solv} Set)[15]	1.2080	1.26172	—	TIP4PEw	
	1.2840	3.95662	—	TIP3P	ΔG_{solv}
	1.2880	4.17787	—	SPC/E	
Li *et al.* ($R_{Mg^{2+}\text{-}O}$ Set)[15]	1.3950	14.91700	—	TIP4PEw	
	1.3950	14.91700	—	TIP3P	$R_{Mg^{2+}\text{-}O}$
	1.3950	14.91700	—	SPC/E	
Li *et al.* (CN Set)[15]	1.3530	9.41798	—	TIP4PEw	
	1.3600	10.20237	—	TIP3P	relative ΔG_{solv} & CN
	1.3600	10.20237	—	SPC/E	
Li & Merz 12-6-4[16]	1.4360	22.36885	1.362	TIP4PEw	
	1.4370	22.57962	1.046	TIP3P	ΔG_{solv},$R_{Mg^{2+}\text{-}O}$,CN
	1.4290	20.93385	0.987	SPC/E	

[a] Main properties considered in parametrization

[b] Includes vdW radii on hydrogens

[c] For Mg^{2+} binding phosphates relative to water

[d] Unpublished results

Table 2

Key features of rigid Mg^{2+}-water interaction energy scans: "contact distance" (σ), minimum energy distance (R), and binding energy (ε). Note: Although an *ab initio* MP2 value is listed in the table for comparison, it is not meant to reflect a meaningful accuracy benchmark, and is not necessarily relevant to the solution properties that are the focus in this work. Nonetheless, as will be seen in later discussion, often the trends in different solution properties are simply related to trends of these simple indexes derived from the Mg^{2+}-water interaction curves, and therefore are useful to aid in the interpretation of the simulation results.

Mg^{2+} Model	Water Model	σ (Å)	R (Å)	ε (kcal/mol)
MP2/6-31++G(d,p)[a]	—	1.45	1.94	−79.2
Åqvist	SPC/E	1.58	1.89	−71.1
Li *et al.* ΔG_{solv}	SPC/E	1.51	1.82	−74.9
Li *et al.* $R_{Mg^{2+}\text{-}O}$	SPC/E	1.67	2.01	−62.6
Li *et al.* CN	SPC/E	1.62	1.94	−66.1
Li & Merz 12-6-4	SPC/E	1.70	2.02	−66.5
Mayaan *et al.*	TIP3P	1.70	2.05	−58.7
Roux	TIP3P	1.54	1.85	−70.8
Allnér *et al.*	TIP3P	1.63	1.96	−63.1
Babu & Lim	TIP3P	1.69	2.03	−59.6
Li *et al.* ΔG_{solv}	TIP3P	1.50	1.80	−73.7
Li *et al.* $R_{Mg^{2+}\text{-}O}$	TIP3P	1.67	2.00	−61.2
Li *et al.* CN	TIP3P	1.62	1.94	−64.7
Li & Merz 12-6-4	TIP3P	1.70	2.03	−65.0
Li *et al.* ΔG_{solv}	TIP4PEw	1.39	1.68	−81.1
Li *et al.* $R_{Mg^{2+}\text{-}O}$	TIP4PEw	1.68	2.02	−58.5
Li *et al.* CN	TIP4PEw	1.62	1.95	−62.4
Li & Merz 12-6-4	TIP4PEw	1.71	2.03	−65.1

[a] Reference QM binding energy scan was based on a rigid TIP3P water geometry and included counterpoise corrections.

Table 3

Summary of structural properties obtained from Mg^{2+}-water pair distribution functions. The first (*i*=1) and second (*i*=2) solvation shell peak maximum and minimum positions $\left(r_i^{max}, r_i^{min}\right)$, their probabilities $\left[g\left(r_i^{max}\right), g\left(r_i^{min}\right)\right]$ and coordination numbers (CN_i) are compared, along with available experimental data. Distances are in units of Å.

Model	Water Model	r_1^{max}	$g(r_1^{max})$	r_1^{min}	$g(r_1^{min})$	CN_1	r_2^{max}	$g(r_2^{max})$	r_2^{min}	$g(r_2^{min})$	CN_2
Åqvist	SPC/E	1.99	24.9	2.49	0.0	6.0	4.18	2.5	4.93	0.7	13.6
Li *et al.* ΔG_{solv}	SPC/E	1.95	22.9	2.44	0.0	6.0	4.14	2.5	4.85	0.7	13.1
Li *et al.* $R_{Mg^{2+}\text{-}O}$	SPC/E	2.08	22.9	2.59	0.0	6.0	4.26	2.3	4.96	0.7	13.7
Li *et al.* CN	SPC/E	2.03	23.8	2.39	0.0	6.0	4.24	2.3	4.9	0.7	13.3
Li & Merz 12-6-4	SPC/E	2.08	26.0	2.48	0.0	6.0	4.22	2.3	4.99	0.8	14.3
Mayaan *et al.*	TIP3P	2.11	22.8	2.58	0.0	6.0	4.37	2.0	5.28	0.8	16.3
Roux	TIP3P	1.97	24.5	2.44	0.0	6.0	4.16	2.3	4.97	0.7	14.0
Allnér *et al.*	TIP3P	2.04	23.5	2.53	0.0	6.0	4.29	2.1	5.32	0.7	16.8
Babu & Lim	TIP3P	2.09	23.1	2.54	0.0	6.0	4.33	2.1	5.32	0.7	16.6
Li *et al.* ΔG_{solv}	TIP3P	1.94	23.8	2.49	0.0	6.0	4.22	2.3	4.99	0.7	14.2
Li *et al.* $R_{Mg^{2+}\text{-}O}$	TIP3P	2.07	23.9	2.49	0.0	6.0	4.28	2.1	5.11	0.7	14.9
Li *et al.* CN	TIP3P	2.03	24.5	2.49	0.0	6.0	4.25	2.2	5.25	0.7	16.1
Li & Merz 12-6-4	TIP3P	2.08	26.4	2.44	0.0	6.0	4.32	2.1	5.18	0.8	16.3
Li *et al.* ΔG_{solv}	TIP4PEw	1.89	17.5	2.60	0.0	6.0	4.09	2.5	4.83	0.6	12.9
Li *et al.* $R_{Mg^{2+}\text{-}O}$	TIP4PEw	2.09	22.3	2.54	0.0	6.0	4.31	2.2	5.03	0.7	13.8
Li *et al.* CN	TIP4PEw	2.04	23.1	2.53	0.0	6.0	4.27	2.3	5.01	0.7	13.8
Li & Merz 12-6-4	TIP4PEw	2.08	26.2	2.49	0.0	6.0	4.26	2.2	4.98	0.8	14.3
Experiment		2.09 ± 0.04[96]				6.0[97]	4.1-4.2[97]				12.0[97]

Table 4

Summary of data extracted from free energy profiles ($R_{Mg^{2+}\text{-}O}$) for inner-sphere water exchange: $\mathbf{R}^{\dagger}$ - transition state distance (Å), **A** - pre-exponential factor (fs^{-1}), $\mathbf{\Delta}G^{\dagger}$ - activation free energy (kcal/mol), $\boldsymbol{k_1}$ - first solvation shell water exchange rate (s^{-1}). Standard deviations come from four consecutive 2 ns segments of data.

Model	Water model	$R^{\dagger}$	A	$\Delta G^{\dagger}$	log(k_1)	k_1
Åqvist	SPC/E	2.88 ± 0.01	0.015	13.9 ± 0.1	3.0 ± 0.1	9.5×10^2
Li *et al.* ΔG_{solv}	SPC/E	2.98 ± 0.01	0.013	12.7 ± 0.3	3.8 ± 0.4	6.4×10^3
Li *et al.* $R_{Mg^{2+}\text{-}O}$	SPC/E	2.76 ± 0.01	0.014	10.9 ± 0.3	5.2 ± 0.4	1.5×10^5
Li *et al.* CN	SPC/E	2.84 ± 0.01	0.014	12.4 ± 0.1	4.1 ± 0.1	1.1×10^4
Li & Merz 12-6-4	SPC/E	2.66 ± 0.02	0.017	10.2 ± 0.3	5.7 ± 0.4	5.5×10^5
Mayaan *et al.*	TIP3P	2.72 ± 0.01	0.015	7.8 ± 0.1	7.5 ± 0.1	2.9×10^7
Roux	TIP3P	2.89 ± 0.00	0.014	12.9 ± 0.1	3.7 ± 0.1	4.8×10^3
Allnér *et al.*	TIP3P	2.75 ± 0.01	0.015	10.9 ± 0.1	5.2 ± 0.1	1.5×10^5
Babu & Lim	TIP3P	2.69 ± 0.02	0.015	8.2 ± 0.1	7.2 ± 0.1	1.5×10^7
Li *et al.* ΔG_{solv}	TIP3P	2.95 ± 0.01	0.012	12.6 ± 0.2	3.9 ± 0.3	7.2×10^3
Li *et al.* $R_{Mg^{2+}\text{-}O}$	TIP3P	2.70 ± 0.00	0.015	9.6 ± 0.1	6.1 ± 0.1	1.3×10^6
Li *et al.* CN	TIP3P	2.78 ± 0.00	0.015	11.6 ± 0.1	4.7 ± 0.1	4.5×10^4
Li & Merz 12-6-4	TIP3P	2.68 ± 0.00	0.017	7.5 ± 0.2	7.7 ± 0.3	5.2×10^7
Li *et al.* ΔG_{solv}	TIP4PEw	3.10 ± 0.01	0.010	8.7 ± 0.1	6.6 ± 0.1	4.2×10^6
Li *et al.* $R_{Mg^{2+}\text{-}O}$	TIP4PEw	2.73 ± 0.01	0.015	9.4 ± 0.2	6.3 ± 0.3	1.9×10^6
Li *et al.* CN	TIP4PEw	2.84 ± 0.01	0.014	11.5 ± 0.1	4.7 ± 0.1	5.1×10^4
Li & Merz 12-6-4	TIP4PEw	2.63 ± 0.00	0.016	8.4 ± 0.2	7.1 ± 0.3	1.1×10^7
Experiment[101]					5.8	$6.7 \pm 0.2 \times 10^5$

Table 5

Scaled infinite dilution diffusion coefficients (× 10^{-5} cm^2/s) and hydrodynamic radii (Å) for the Mg^{2+} parameters and the respective solvent viscosities (× 10^{-4} $kgm^{-1}s^{-1}$). D_o, η and r are D_o^{sim}, η^{sim} and r^{sim} (Table S5) re-scaled by $\frac{D_o^w}{\tilde{D}_o^w}$ (see discussion in Methods) to correct for errors in the diffusion coefficients of the water models.

Model	Water model	D_o	η	r
Åqvist	SPC/E	0.741 ± 0.057	9.23 ± 0.36	3.19
Li *et al.* ΔG_{solv}	SPC/E	0.736 ± 0.052	9.16 ± 0.28	3.24
Li *et al.* $R_{Mg^{2+}\text{-}O}$	SPC/E	0.735 ± 0.052	9.67 ± 0.23	3.07
Li *et al.* CN	SPC/E	0.723 ± 0.052	9.81 ± 0.21	3.08
Li & Merz 12-6-4	SPC/E	0.748 ± 0.044	9.19 ± 0.24	3.18
Mayaan *et al.*	TIP3P	0.779 ± 0.052	9.18 ± 0.11	3.05
Roux	TIP3P	0.817 ± 0.049	7.64 ± 0.11	3.50
Allnér *et al.*	TIP3P	0.802 ± 0.068	8.24 ± 0.27	3.30
Babu & Lim	TIP3P	0.798 ± 0.057	8.79 ± 0.28	3.11
Li *et al.* ΔG_{solv}	TIP3P	0.790 ± 0.065	8.32 ± 0.10	3.32
Li *et al.* $R_{Mg^{2+}\text{-}O}$	TIP3P	0.771 ± 0.057	9.38 ± 0.10	3.02
Li *et al.* CN	TIP3P	0.783 ± 0.059	9.09 ± 0.29	3.07
Li & Merz 12-6-4	TIP3P	0.813 ± 0.059	8.59 ± 0.41	3.13
Li *et al.* ΔG_{solv}	TIP4PEw	0.744 ± 0.051	8.70 ± 0.21	3.37
Li *et al.* $R_{Mg^{2+}\text{-}O}$	TIP4PEw	0.779 ± 0.061	7.97 ± 0.18	3.52
Li *et al.* CN	TIP4PEw	0.740 ± 0.050	8.77 ± 0.10	3.36
Li & Merz 12-6-4	TIP4PEw	0.801 ± 0.052	8.01 ± 0.22	3.40
Experiment		0.706[102]	8.903[103]	